Atmospheric Research 197 (2017) 132–149

Contents lists available at ScienceDirect

Atmospheric Research

journal homepage: www.elsevier.com/locate/atmosres

Spatiotemporal variability of temperature and precipitation in Gansu Province (Northwest China) during 1951–2015

Xiaohu Wen[a], Xiaoqing Wu[b], Meng Gao[b,*]

[a] Northwest Institute of Eco-Environment and Resources, CAS, Lanzhou, Gansu 730000, China
[b] Key Laboratory of Coastal Environmental Processes and Ecological Remediation, Yantai Institute of Coastal Zone Research, CAS, Yantai, Shandong 264003, China

ARTICLE INFO

Keywords:
Climate extreme
Trend
Spatial pattern
Periodicity
Atmospheric circulation

ABSTRACT

Climate change is potentially challenging the sustainable development in many parts of the world, especially the semi-arid and arid regions on the earth. Northwest China (NWC) is one of the most arid areas in East Asia, and Gansu Province is located at the important climate transition zone in NWC. Spatiotemporal variability of both temperature and precipitation were analyzed based on the daily observation dataset at 29 meteorological stations over Gansu during 1951–2015. The Mann–Kendall trend test was utilized to detect monotonic trends in extreme climate indices, mean temperature, and total precipitation. The results revealed that the warming trends were statistically significant at most stations in Gansu, especially at the high altitude stations; however, the change trends in annual and seasonal precipitation over Gansu were not significant as expected. Furthermore, the 29 stations were spatially grouped using hierarchical clustering method. The regional-averaged temperature anomalies also showed a significant warming trend beginning at the end of 1970s. Spatial variations were also observed in the annual and seasonal precipitation over Gansu. In general, precipitation increased in the western part of Gansu while decreased in the eastern part. Additionally, the wavelet analyses revealed that the teleconnection between large scale circulation and summer precipitation varied not only from region to region, but also was different at different time scale and different time periods. Analysis of large-scale atmospheric circulation changes showed that a strengthening anticyclonic circulation, increasing geopotential height and rapid warming over the Eurasian continent were considered to be attributable to climate change in Gansu and even in NWC.

1. Introduction

Recent studies have revealed a significant global warming trend during the past century (Easterling et al., 2000; Yan et al., 2002; Brohan et al., 2006; Gay-Garcia et al., 2009; IPCC, 2014). Global warming in turn leads to a higher moisture content in the atmosphere and then potentially affects the global hydrological cycle (Trenberth, 2011). It was estimated that global land precipitation increased by approximately 2% over the 20th century (New et al., 2001), resulting a slight overall increase in global river runoff and in average soil moisture (Huntington, 2006). For decades, global changes in temperature and precipitation have been extensively investigated using long-term observational data (Klein Tank et al., 2002; Alexander et al., 2006). Evident regional differences in the temperature and precipitation change on global scale were also observed (Houghton et al., 2001; Alexander et al., 2006). The Intergovernmental Panel on Climate Change (IPCC) suggested that it was necessary to study climate change on regional and local scales, which was of particular importance to nations and economic groups to response climate change (IPCC, 2007).

Semi-arid and arid regions of the world are often considered as being particularly vulnerable to climate change due to warming and drying (Sarr, 2012; Revi et al., 2015). Gansu Province (32°31′–42°57′ N and 92°13′–108°46′ E) is located in Northwest China (NWC), one of the most arid areas in East Asia. Regarding the area (0.45 million km^2) across the province level in China, Gansu is merely a moderate-sized administrative province, but stretches over 1400 km from southeast to northwest (Fig. 1). Gansu Province covers multiple climate types from humid (in southwest) to semi-humid, and then to semi-arid and arid. Generally, the summer is warm and hot while the winter is cool and cold. Some high altitude areas of Gansu also exhibit a subarctic climate, and the snow line can be as high as 5500 m above sea level. The annual total precipitation ranges from 40 mm to 800 mm with a drying gradient from southeast to northwest (H.X. Wang et al., 2013; H.J. Wang et al., 2013). The spatial variabilities in precipitation are attributable to the combing effects of monsoon system and topography. Besides spatial variabilities, there are significant temporal variabilities in the

* Corresponding author.
E-mail address: mgao@yic.ac.cn (M. Gao).

http://dx.doi.org/10.1016/j.atmosres.2017.07.001
Received 2 November 2016; Received in revised form 27 June 2017; Accepted 3 July 2017
Available online 04 July 2017
0169-8095/

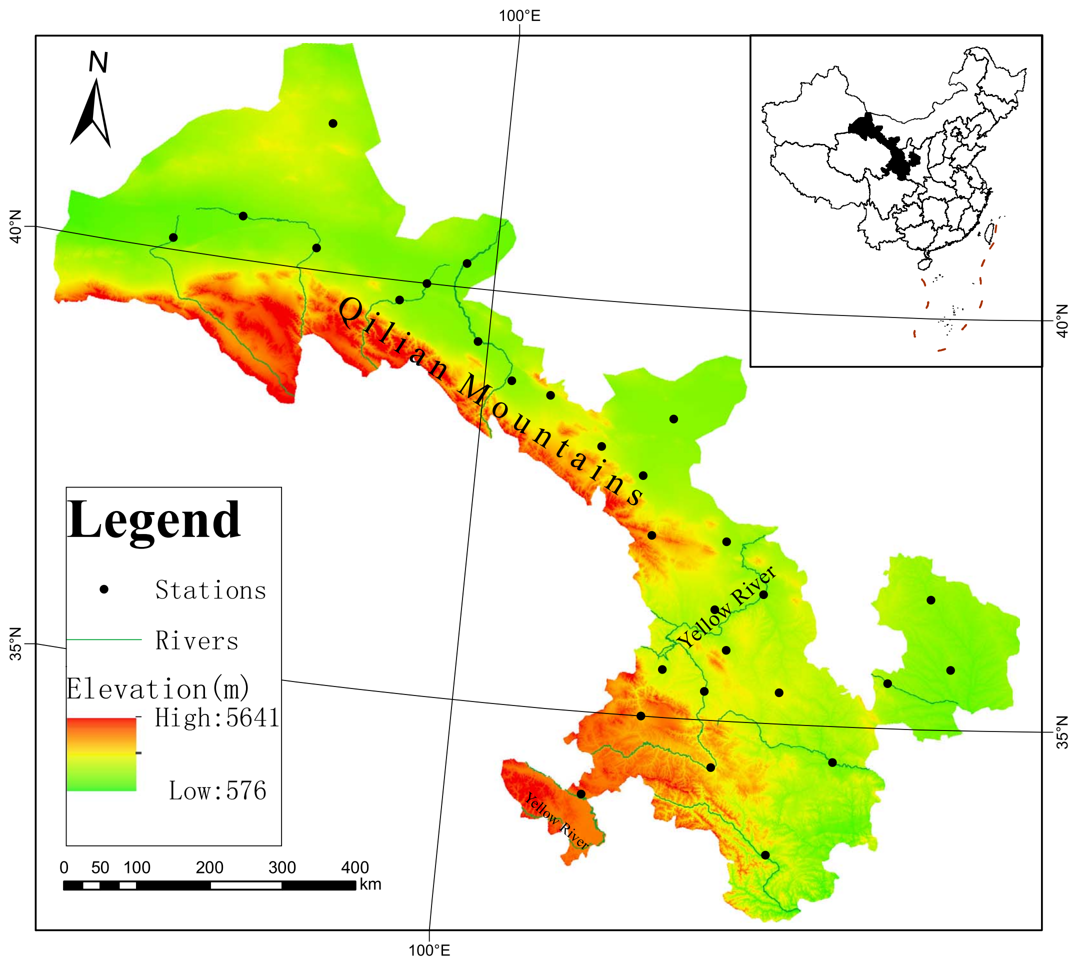

Fig. 1. Map of Gansu Province showing the topography and locations of the selected 29 meteorological stations.

precipitations in Gansu. Within each year, most of the precipitation is delivered in summer, and there are also significant inter-annual and inter-decadal variability in the precipitation. The limited precipitation is extremely critical to the irrigated agriculture and oasis eco-environment in Gansu. However, spatiotemporal variability in precipitation negatively affects the human use of water resources and limits the socio-economic development in Gansu, especially in the central and western parts of Gansu. Additionally, Gansu lies among the Tibetan Plateau, the Mongolian Plateau, and the Loess Plateau. The vast majority of its land is higher than 1000 m above the sea level with a mountainous landscape (Fig.1). Mountainous and highland regions are especially sensitive and vulnerable to extreme climate change (Beniston et al., 1997; Diaz et al., 2003). Due to climate change, the frequency and intensity of climate extremes, such as floods, droughts and heat waves, have significantly increased (IPCC, 2012). Because of low level of vegetation cover, heavy rainfalls easily cause natural hazards such as floods and mudslides in mountainous areas in Gansu. On August 8th 2010, a severe mudslide caused by heavy rainfall and flooding occurred in Zhugqu county, southern Gansu. It left 1557 people dead and 208 missed, and the estimated economic loss reached 13.3 billion CNY (about 1.94 billion USD) (Xinhua News, 2015). Therefore, it is worthy to study the changes in climate extremes in Gansu under the background of global climate change.

In an administrative division, the Gansu Province belongs to NWC; however, in a traditional natural division, the Gansu Province is a region covering all three zones (Arid Northwest China, Monsoon East China and Tibetan Plateau) or four zones (Arid Northwest China, Monsoon North China, Monsoon South China and Tibetan Plateau). Great efforts have been made to characterize the spatiotemporal variability of temperature and precipitation, especially the change of climate extremes in NWC. H.X. Wang et al. (2013) and H.J. Wang et al. (2013) studied the spatial distribution and temporal trends of the mean precipitation and extremes in the NWC including the Xinjiang and the western part of Gansu, during 1960–2010. Li et al. (2013) compared the temperature and precipitation changes in three different landscapes, mountain, oasis, and the desert areas, in NWC. Li et al. (2016) identified the possible causes of the significant increasing trend of precipitation in the NWC during 1960–2010. Yang et al. (2017) analyzed the

Table 1
List of observation stations with WMO (World Meteorological Organization) ID, latitude, longitude, and altitude (m).

WMO ID	Station name	Latitude (N)	Longitude (E)	Altitude (m)
52,323	Mazongshan	41°48′	97°02′	1770
52,418	Dunhuang	40°09′	94°41′	1139
52,424	Gauzhou	40°32′	95°46′	1170
52,436	Yumen	40°16′	97°02′	1526
52,446	Dingxin	40°18′	99°31′	1177
52,447	Jinta	40°00′	98°54′	1270
52,533	Jiuquan	39°46′	98°29′	1477
52,546	Gaotai	39°22′	99°50′	1332
52,652	Zhangye	38°56′	100°26′	1482
52,661	Shandan	38°48′	101°05′	1764
52,674	Yongchang	38°14′	101°58′	1976
52,679	Wuwei	37°55′	102°40′	1531
52,681	Minqin	38°38′	103°05′	1367
52,787	Wushaoling	37°12′	102°52′	3045
52,797	Jingtai	37°11′	104°03′	1630
52,884	Gaolan	36°21′	103°56′	1668
52,895	Jingyuan	36°34′	104°41′	1398
52,983	Yuzhong	35°52′	104°09′	1874
52,984	Linxia	35°35′	103°11′	1917
52,986	Lintao	35°21′	103°51′	1893
52,996	Huajialing	35°23′	105°00′	2450
53,821	Huanxian	36°35′	107°18′	1255
53,915	Pingliang	35°33′	106°40′	1346
53,923	Xifeng	35°44′	107°38′	1421
56,074	Maqu	34°00′	102°05′	3471
56,080	Hezuo	35°00′	102°54′	2910
56,093	Minxian	34°26′	104°01′	2315
56,096	Wudu	33°24′	104°55	1079
57,014	Maiji	34°34′	105°52	1085

spatiotemporal variations of precipitation at different timescales and detected different trends in precipitations at different river basins. In the above studies, only the western Gansu was included in the study area of NWC, while the eastern part was not included. Han et al. (2016) found that the precipitation decreased in the eastern region of NWC, including Gansu and Shaanxi provinces. Besides research about climate change in NWC, the changes in temperature and precipitation in central and western Gansu also appeared in studies about climate change on Loess Plateau (China). Li et al. (2010) analyzed the trends of extreme temperature and precipitation on Loess Plateau, and found that extreme precipitation events did not change significantly but extreme temperature events became more severe and frequent. Wang et al. (2012, 2016) investigated the change trends of annul mean temperature and annual total precipitation, and temperature and precipitation extremes on Loess Plateau, respectively. Sun et al. (2016) also assessed the annual and decadal trends of temperature and precipitation extremes over Loess Plateau. In these previous studies, either the western or the central and eastern parts of Gansu was included; however, the spatiotemporal variabilities in temperature and precipitation over the whole province have not been covered.

The objective of this study is to investigate the spatiotemporal variability of temperature and precipitation synthetically based on daily observations at 29 meteorological stations in Gansu Province. Statistical analyses are firstly applied to the mean and extreme sequences of temperature and precipitation, and then the 29 stations are divided into 6 different groups using spatial clustering method. For each Division, the regionally averaged precipitation time series from 1951 to 2015 are computed and analyzed. In addition, the relationship between spatiotemporal variability of summer total precipitation and large scale atmospheric circulation patterns are also discussed.

2. Data and methods

2.1. Daily meteorological dataset

The daily meteorological dataset was provided by the Climate Data Center of the China Meteorological Administration (CMA), and the data quality was also controlled by the NMIC (Qian and Qian and Lin, 2005).There are 35 meteorological stations in Gansu in the original dataset, but 6 of them are excluded for further statistical analysis due to data incompleteness. The time series of daily precipitation, maximum temperature, mean temperature, and minimum temperature records at the remaining 29 meteorological stations were extracted from the dataset, respectively (Fig. 1). Of these stations, most were established in 1950s, and the detailed information about the 29 stations was listed in Table 1. For temperature, the annual, spring (March to May), summer (June to August), autumn (September to November) and winter (December to February) temperature means were calculated by the averaging the daily mean temperature. For precipitation, the annual precipitation time series at each station was calculated by summing up the daily precipitation in every year, while the seasonal precipitation was calculated in a similar way. Years with > 15 days missing, and months with > 3 days missing, were considered to be of poor quality and were masked here with Null. To facilitate trend analysis and comparison between the stations, we calculated the temperature and precipitation anomalies by subtracting the long term averages during 1961–1990.

2.2. Extreme climate indices

Extreme climate indices, including 11 extreme temperature indices (*TXx*, *TNx*, *TXn*, *TNn*, *TN10p*, *TX10p*, *TN90p*, *TX90p*, *DTR*, *WSDI*, *CSDI*) and 4 extreme precipitation indices (*RX1day*, *RX5day*, *CDD*, *PRCPTOT*),

Table 2
Definitions of extreme temperature and precipitation indices used in this study.

ID	Indicator name	Definition	Units
TXx	Max Tmax	Monthly maximum value of daily max temperature	°C
TNx	Max Tmin	Monthly maximum value of daily min temperature	°C
TXn	Min Tmax	Monthly minimum value of daily max temperature	°C
TNn	Min Tmin	Monthly minimum value of daily min temperature	°C
TN10p	Cool nights	Percentage of time when daily min temperature < 10th percentile	%
TX10p	Cool days	Percentage of time when daily max temperature < 10th percentile	%
TN90p	Warm nights	Percentage of time when daily min temperature > 90th percentile	%
TX90p	Warm days	Percentage of time when daily max temperature > 90th percentile	%
DTR	Diurnal temperature range	Monthly mean difference between daily max and min temperature	°C
WSDI	Warm spell duration indicator	Annual count when at least 6 consecutive days of max temperature > 90th percentile	days
CSDI	Cold spell duration indicator	Annual count when at least 6 consecutive days of min temperature < 10th percentile	days
RX1day	Max 1-day precipitation amount	Monthly maximum 1-day precipitation	mm
RX5day	Max 5-day precipitation amount	Monthly maximum consecutive 5-day precipitation	mm
CDD	Consecutive dry days	Maximum number of consecutive days when precipitation < 1 mm	days
PRCPTOT	Annual total wet-day precipitation	Annual total precipitation from days ≥ 1 mm	mm

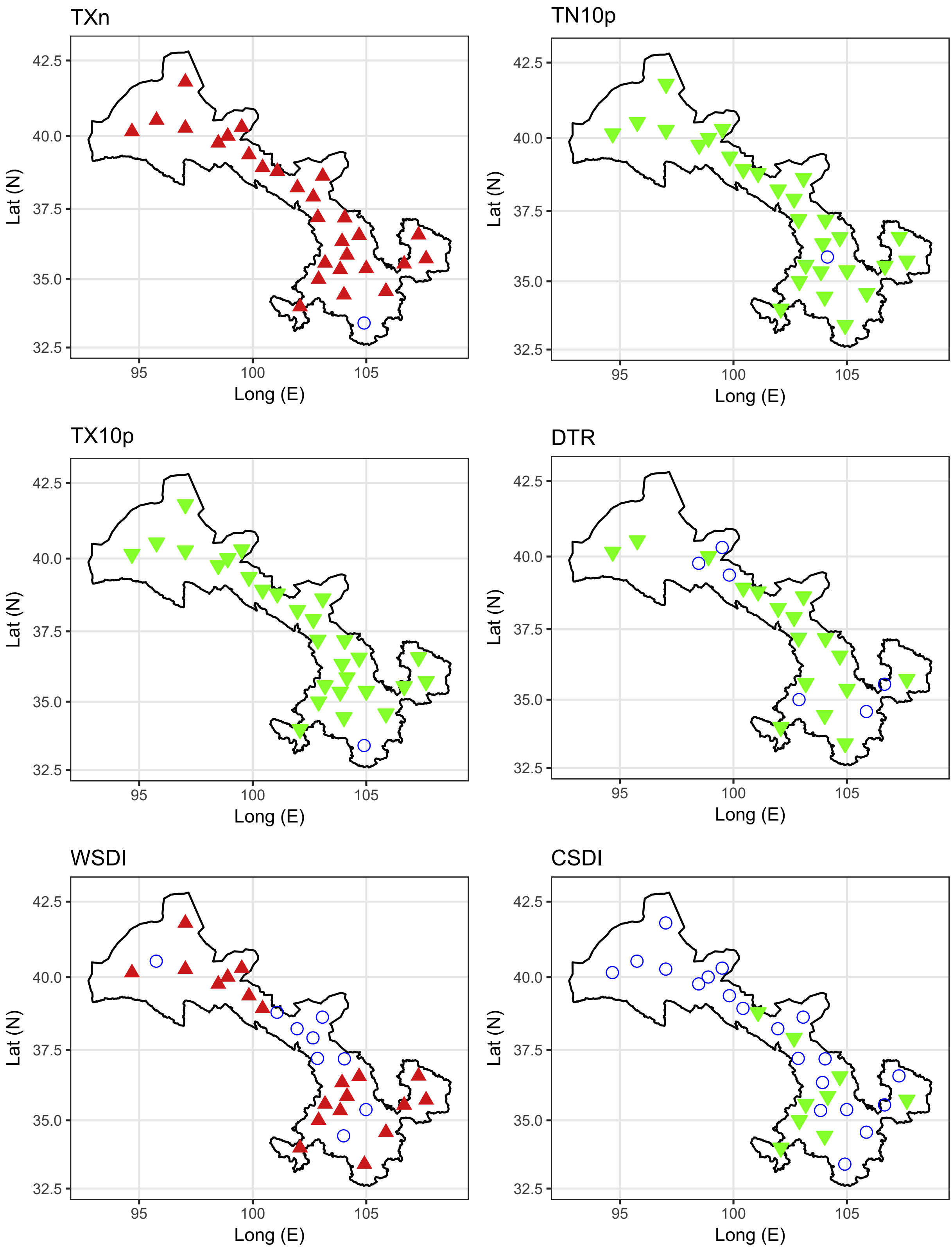

Fig. 2. Spatial patterns of Mann–Kendall trends for 6 extreme temperature indices (*TXn*, *TN10p*, *TX10p*, *DTR*, *WSDI*, *CSDI*) over Gansu Province during 1951–2015. The upward (or downward) pointing triangles represent significant (5% level) positive (or negative) trends, while circles represent nonsignificant trends.

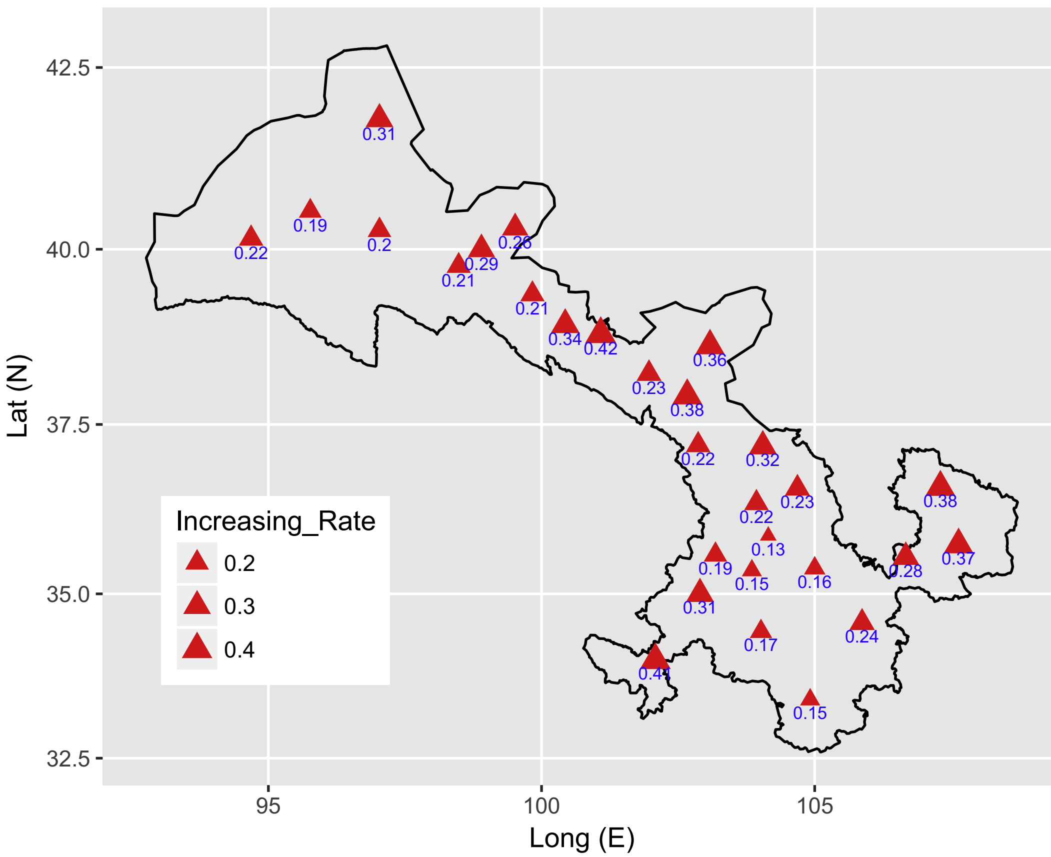

Fig. 3. Linear trends of annual mean temperature per decade at 29 meteorological stations over Gansu Province.

were used in this study as recommended by the CCl/CLIVAR/JCOMM Expert Team on Climate Change Detection and Indices (Table 2). The other 12 climate extreme indices those were not suitable to the varied climate in Gansu Province were not selected. These indices have been widely used to assess the changes in climate extremes (Klein Tank et al., 2006; Li et al., 2010; You et al., 2011; Limsakul and Singhruck, 2016; Panda et al., 2016). The description and definition of these extreme climate indices could also be found in Alexander et al. (2006). These selected indices were calculated based on the daily temperature and precipitation sequences using the R-package "*climdex.pcic*" (https://cran.r-project.org/web/packages/climdex.pcic/).

2.3. Large-scale atmospheric circulation

The temporal variability of summer rainfall in NWC is tightly associated with large scale climate patterns in the Northern Hemisphere (Ding and Wang, 2005; Huang et al., 2011; Chen and Huang, 2012). Specifically, it was found that East Asian summer monsoon determined the spatiotemporal variability of summer rainfall over China (Ding and Chan, 2005; Zhao and Zhou, 2009). The annual East Asian summer monsoon index (EASMI) time series was collected by Professor Li J.P. and could be directly downloaded from the following website (http://ljp.gcess.cn/dct/page/65577). The Asian monsoon system is also strongly affected by El Niño Southern Oscillation (ENSO) that has the greatest impact on the year-to-year variability of the global climate (Tanaka, 1997; Wang et al., 2000). Because ENSO is generally at its peak during November–January (Trenberth, 1997), its effect on extreme precipitation is in the following summer (Lin and Lu, 2009). In this study, Southern Oscillation Index (SOI) was used to quantify ENSO. The average of monthly SOI from November to next January was calculated generating the SOI series from 1950 to 2014. Tan and Shao (2016) also found that Eastern Atlantic/Western Russia (EAWR) pattern, which was one of the prominent teleconnection patterns that affected Eurasia (Lim, 2015), significantly influenced summer precipitation in NWC. These two atmospheric circulation indices, SOI and EAWR, were both available at the National Oceanic and Atmospheric Administration (http://www.esrl.noaa.gov/psd/data/climateindices). To further assess the changes in large scale atmospheric circulation, monthly mean geopotential height and wind fields at 500 hPa and 850 hPa that were derived from National Centers for Environmental

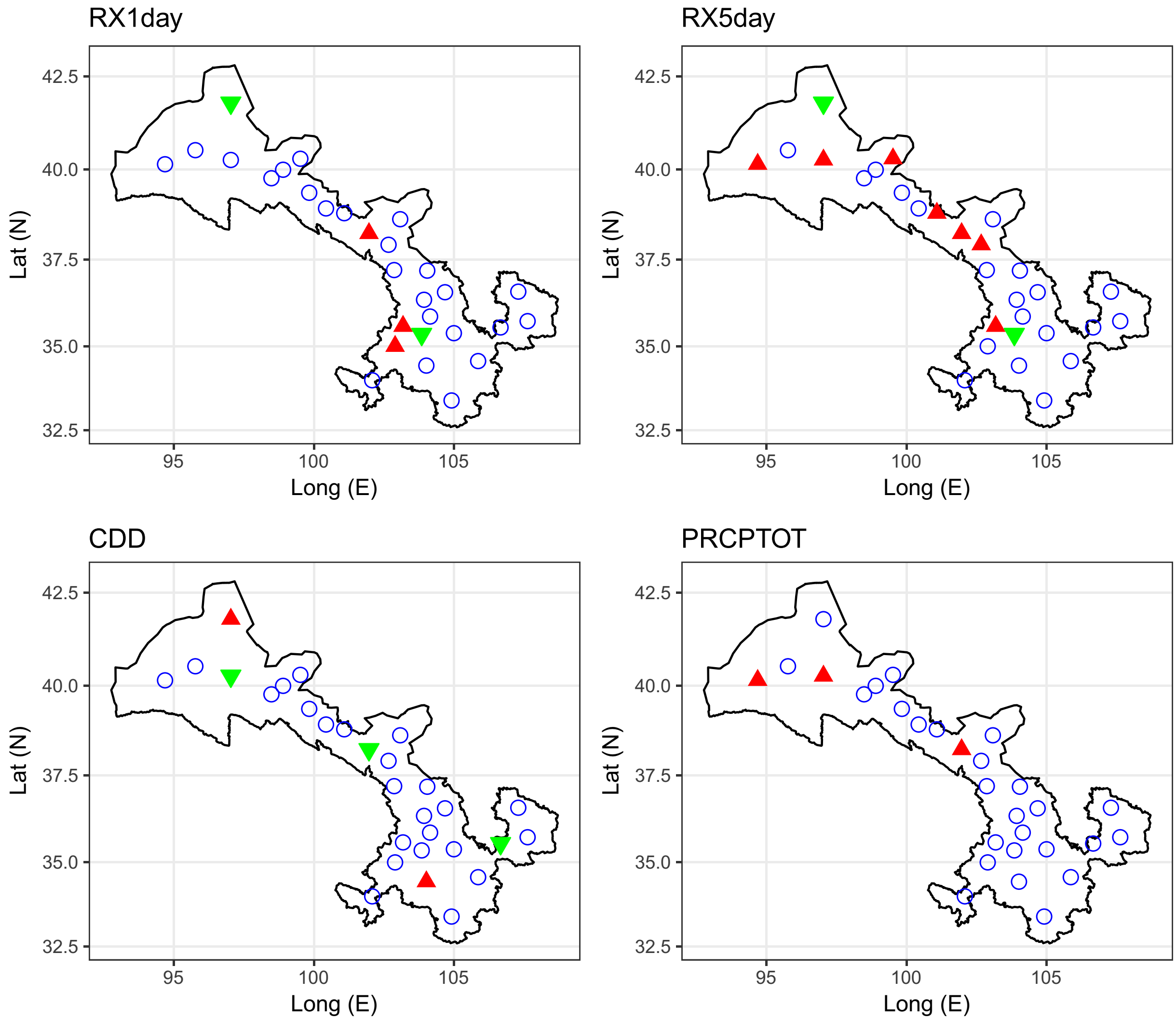

Fig. 4. Spatial patterns of Mann–Kendall trends for 4 extreme precipitation indices (*RX1day*, *RX5day*, *CDD*, *PRCPTOT*) over Gansu Province during 1951–2015. The upward (or downward) pointing triangles represent significant (5% level) positive (or negative) trends, while circles represent nonsignificant trends.

Prediction/National Center for Atmospheric Research (NCEP/NCAR) reanalysis data was also analyzed. The long term average in summer and winter for two periods 1956–1980 and 1981–2015 were calculated, respectively, then former were subtracted from the latter (new minus old) to represent the change in circulation between the two periods. The NCEP/NCAR dataset is available at http://www.cdc.noaa.gov.

2.4. Statistical analysis methods

The statistical significance of monotonic trend in extreme climate indices, mean temperature, and total precipitation time series was evaluated by the rank-based Mann–Kendall (M-K) trend test (Mann, 1945; Kendall, 1970). To reduce the impact of serial correlations, all time series have been prewritten before trend detection (Burn and HagElnur, 2002). In this study, the R-package "*Kendall*" was used to implement M-K trend test (https://cran.r-project.org/web/packages/kendall/). Linear regression analysis was further applied to quantify the change rate of mean temperature per decade (slope of the linear trend) by way of least squares. The 29 meteorological stations were then spatially grouped into different divisions using the agglomerative hierarchical clustering method based on the characteristics of temperature and precipitation, respectively (Hosking and Wallis, 1997). For each Division, the regionally averaged annual and seasonal mean temperature and total precipitation were computed. The periodic features of annual and seasonal precipitation as well as climate indices were also analyzed using the continuous wavelet transform (CWT), while the correlation relationship between atmospheric circulation indices (EASMI, SOI, EAWR) and annual or seasonal precipitation was revealed using cross wavelet transform (XWT) (Torrence and Webster, 1999; Grinsted et al., 2004).

3. Results

3.1. Changes in temperature and precipitation

The spatial distribution patterns of change trends for 6 extreme temperature indices (*TXn*, *TN10p*, *TX10p*, *DTR*, *WSDI*, *CSDI*) were shown in Fig. 2. It was found that the minimum temperature increased

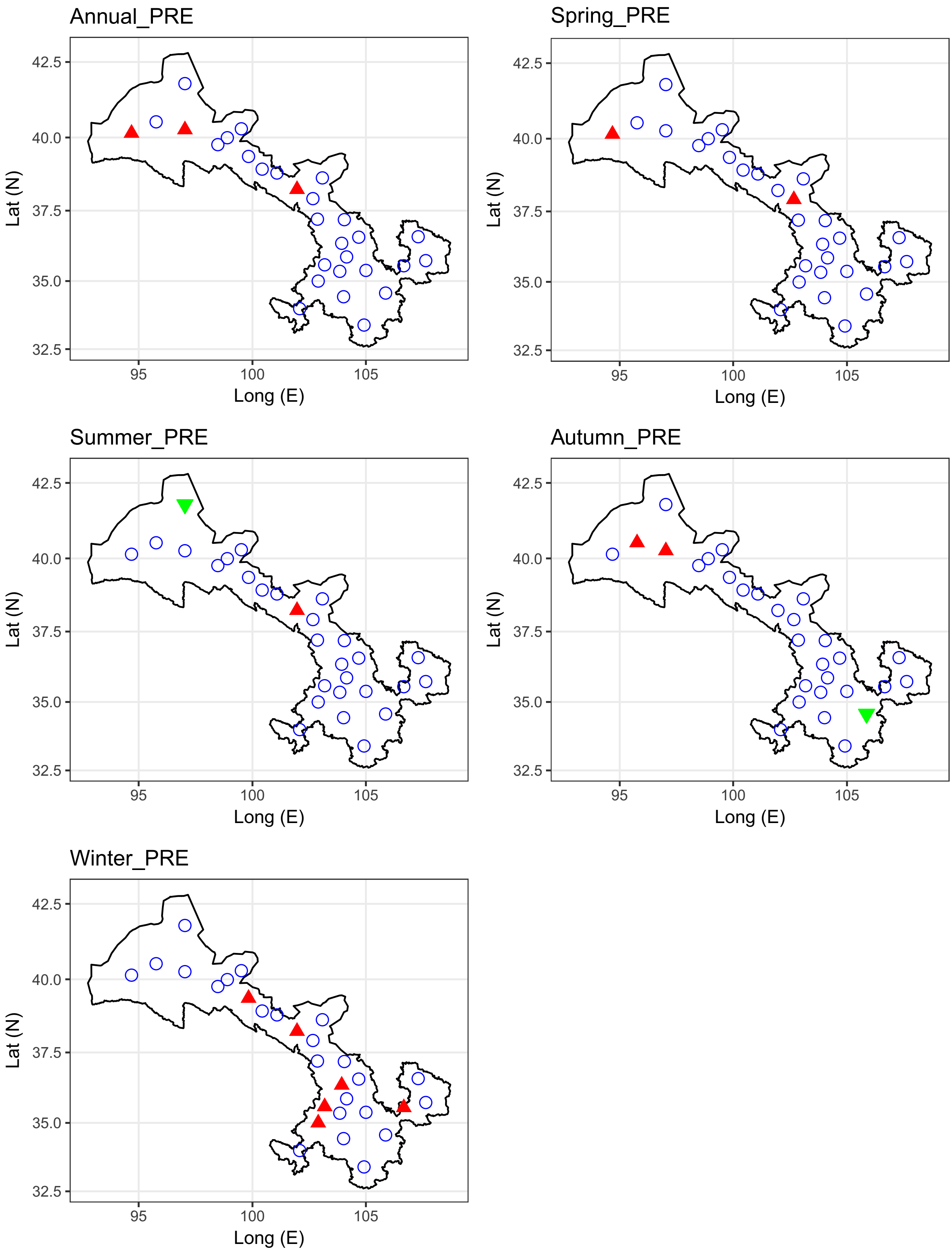

Fig. 5. Spatial patterns of Mann–Kendall trends for annual and seasonal total precipitation over Gansu Province during 1951–2015. The upward (or downward) pointing triangles represent significant (5% level) positive (or negative) trends, while circles represent nonsignificant trends.

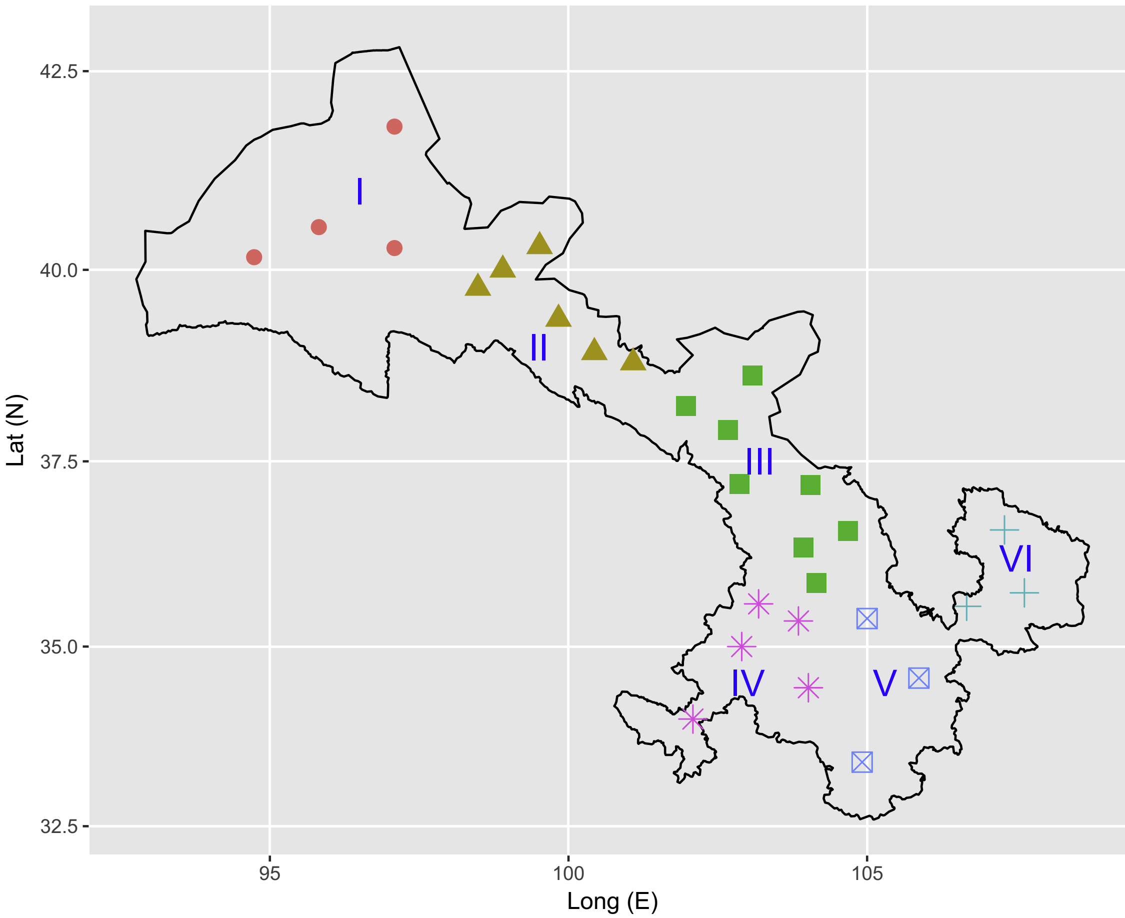

Fig. 6. Temperature and precipitation division based on hierarchical clustering method in Gansu from 1951–2015.

but the cool days, cool nights, and diurnal temperature range decreased (5% significance level) at most stations. The increasing trends of other 5 extreme temperature indices (*TXx*, *TNx*, *TNn*, *TN90p*, *TX90p*) were not shown as figures here, because the increasing trends for these 5 indices were all significant at 5% level. It indicated that both maximum temperature and warm days increased during 1951–2015. The warming trend was consistent with rapid warming trend over China found in some previous literatures (Xu et al., 2011; You et al., 2011). The linear trends of annual mean temperature were illustrated in Fig. 3. Annual mean temperature anomalies at all 29 stations showed a significant (5% level) positive trend over Gansu. Owing to topographical complexity, the increasing rate of annual mean temperature was spatially varied ranging from 0.13 to 0.42 °C/decade during 1951–2015, which was consistent with the warming trend (0.27 °C/decade) during 1961–2003 over China (You et al., 2011) but was much stronger than the global warming rate 0.19 °C/decade (Hansen et al., 2006).

Fig. 4 illustrated the trends of 4 extreme precipitation indices (*RX1day*, *RX5day*, *CDD*, *PRCPTOT*). For *RX1day*, significant (5% level) positive or negative trends were detected only at 2 or 1 stations, respectively. These two numbers become 4 and 2, when the trend of extreme precipitation index *RX1day* was examined. M-K trend test for *CDD* demonstrated that only two stations had significant decreasing trends at 5% level. For *PRCPTOT*, only one station at central Gansu showed significant positive trend (Fig. 4). The above results indicated that the spatial patterns of change trends of the 4 extreme precipitation indices were inconsistent. To further investigate the precipitation change in Gansu, the trends of annual and seasonal total precipitation at 29 stations were shown in Fig. 5. Analogously, nonsignificant trends were detected at most stations; however, a few of positive trends and only one negative trend in summer total precipitation was also detected. It was concluded that the spatial variability in climate change was not easily detected at station level; therefore, it is necessary to divide Gansu into small divisions with similar climate features.

3.2. Climate division and regional patterns of temperature and precipitation

The 29 stations were spatially grouped using agglomerative hierarchical clustering method based on temperature (extreme and mean temperature) and precipitation (extreme and total precipitation) indices, respectively. We define each group as a Division. The optimal group numbers were determined according to the difference between the average of between-group correlations and within-group correlation. From Fig. 6, we found that the results of spatial grouping based on either temperature indices or precipitation indices were exactly the same with 6 Divisions indicting the same spatial patterns of temperature and precipitation in Gansu.

The annual and seasonal (summer and winter) time series of regionally averaged temperature anomalies relative to the 1961–1990 mean value for 6 Divisions were shown in Fig. 7. It was observed that overall warming in Gansu Province started at the end of 1970s and

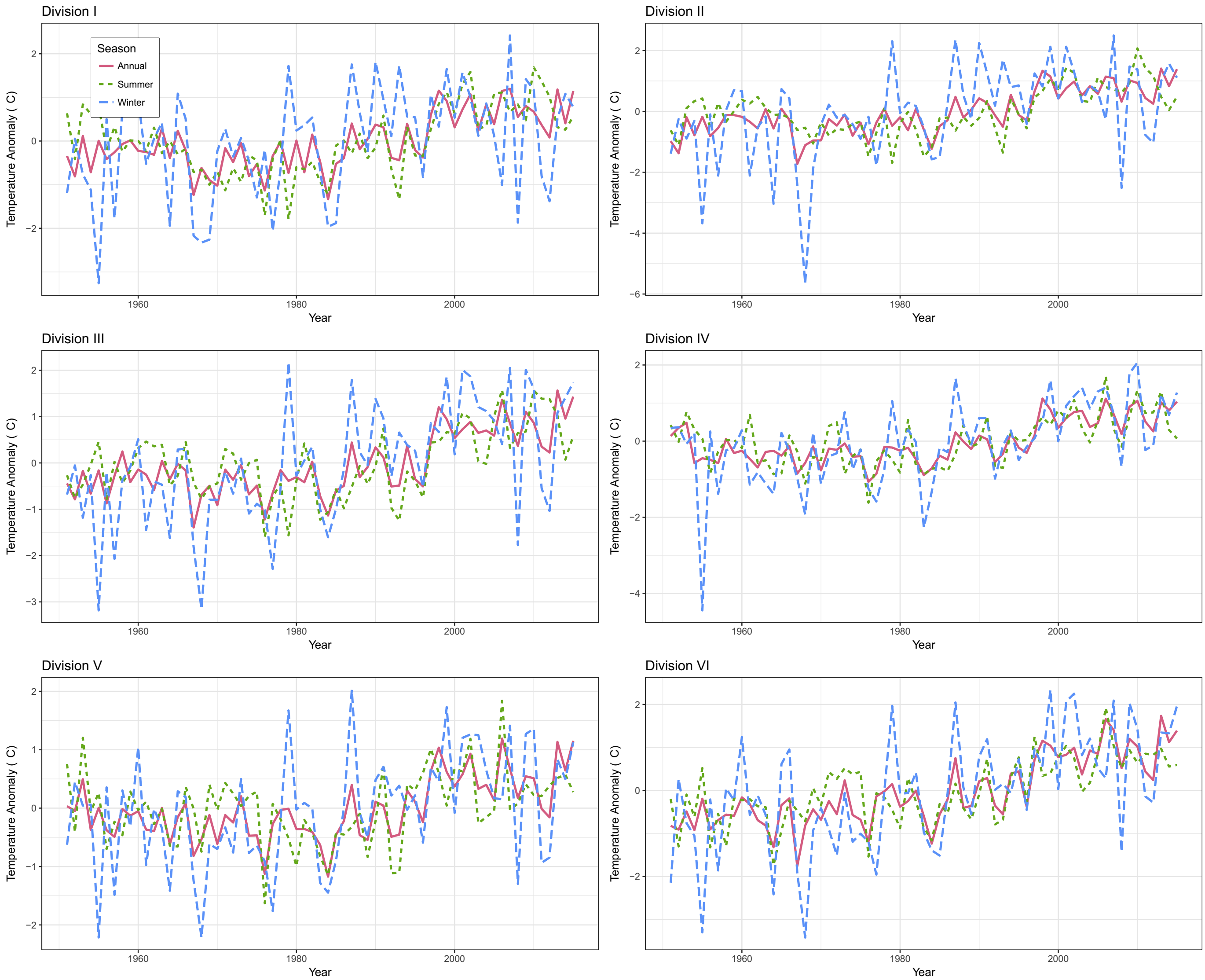

Fig. 7. Annual and seasonal (summer and winter) time series of regionally averaged temperature anomalies in 6 Divisions.

accelerated after 1990s. From Fig. 7, we also found that the winter mean temperature had the strongest inter-annual variations, while the summer mean temperature was more or less correlated with annual mean temperature. Figs. 8–10 illustrated the annual and seasonal (summer and winter) time series of regionally averaged precipitation anomalies as well as the linear trends and the 5-year moving averages. Generally, annual total precipitation slightly increased in Division I and II, which were located near the western part of northwest China, but decreased in Division III-VI. This result was consistent with that in Han et al., (2016). Summer total precipitation mainly increased in Division I but decreased in Division II, III, and VI. Winter total precipitation mainly increased in Division II and IV but decreased in Division I and V. Similar inter-annual and inter-decadal variabilities were observed in annual and summer total precipitation time series, because most precipitation was delivered in summer. In the next subsection, the temporal variability of regionally averaged summer total precipitation would be analyzed, and the teleconnection between summer precipitation and climate indices would be identified.

3.3. Inter-annual variations of climate indices and summer precipitation

The periodic features of climate indices and regionally averaged summer precipitation were analyzed by using the continuous wavelet transform (CWT). Fig. 11 showed the continuous wavelet power spectra for the time series of EASMI, SOI (winter), and EAWR (summer). The significant wavelet power spectra of EASMI (Fig. 11a) were 2–7 year and 14–16 year modulation of variation, which existed during 1970–2005 and 1965–1980, respectively. For winter SOI, the power was broadly distributed, with peaks 2–4 years and 4–7 years. The 95% significance level regions indicated intervals of higher variance from 1970 to 1990 with a 2–4 year cycle and from 1975–2000 with a 4–7 year cycle (Fig. 11b). Meanwhile, there existed nonsignificant (95% significance level) 4–7 year cycle and 14-year cycle during 1965–1975 and 1965–2015, respectively. Continuous wavelet power spectrum for summer EAWR (Fig. 11c) showed significant wavelet power at 7–14 years during 1972–2000. From 1951–1975, it also showed a 4–6 year cycle. For the above three climate indices, a nonsignificant

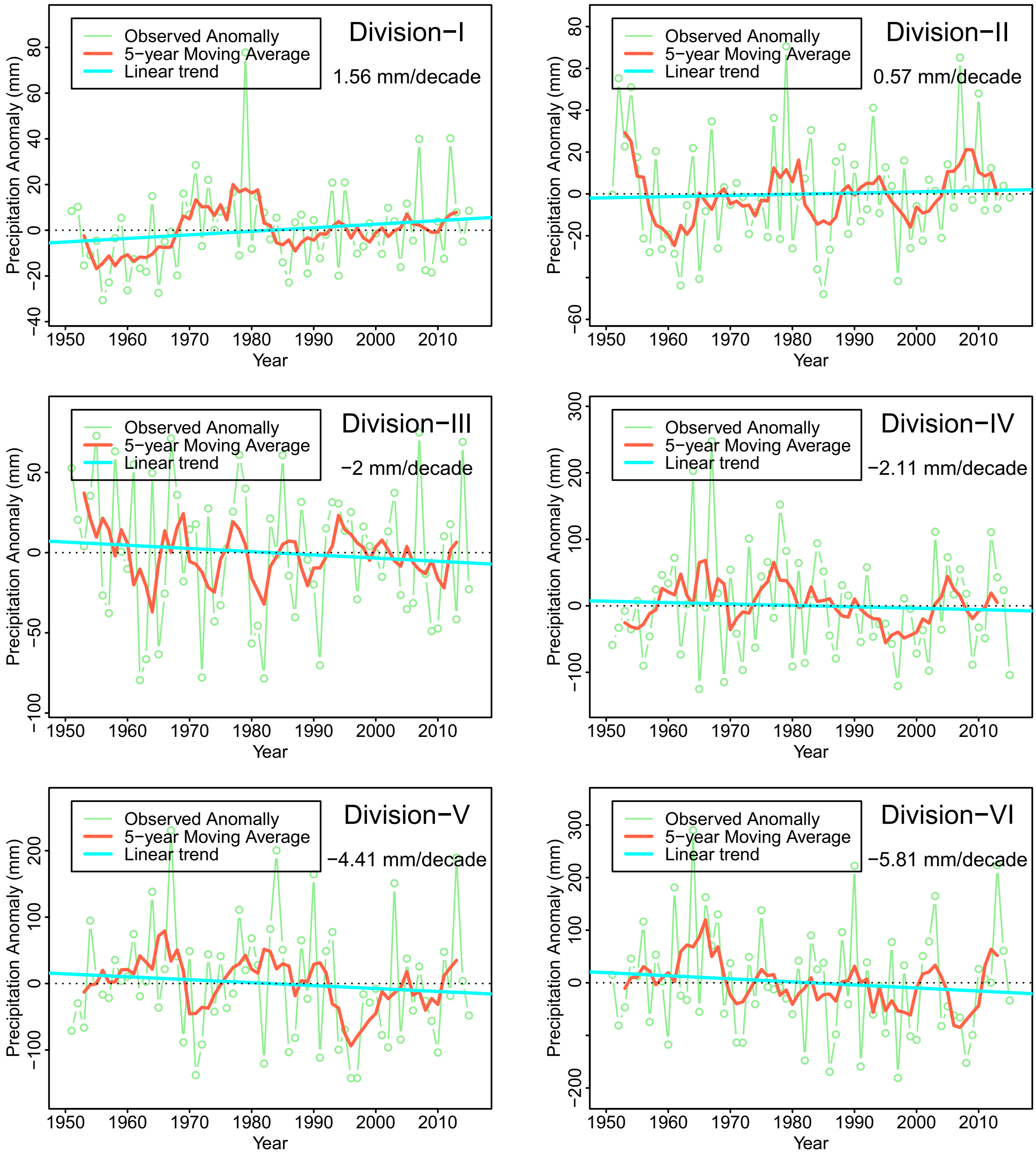

Fig. 8. Time series of regionally averaged annual total precipitation anomalies (circles) as well as the linear trends (straight lines) and the 5-year moving averages (the smoother lines).

2–4 years cycle was found from 2005–2015. Wavelet analysis for summer precipitation in Division I-VI did not generate similar continuous wavelet power spectrum (Figs. 12 and 13) indicting that the inter-annual variability of summer precipitation in these 6 Divisions were not highly correlated. In Division I, there was a 2–4 year cycle during 1975–1985. In Division II, 2–7 year cycle appeared during 1972–1995. In Division III, 7–11 year cycle peaked during 1965–1995. In Division IV, wavelet power spectrum showed 2–4 year, 4–7 year modulations of variation, which existed during 1965–1985 and 1975–1990, respectively. In Division V, 2–7 year cycle appeared during 1975–1995. In Division VI, continuous wavelet power spectrum showed significant wavelet power at 2–4 years during 1955–1975.

Next, the correlation between summer precipitation in each Division and climate indices was revealed using cross wavelet transform (XWT). In total, we had 6 Divisions and 3 climate indices resulting in 18 XWTs, but were not all illustrated here. Fig. 14(a) illustrated the cross-wavelet transform between EASMI and summer precipitation in Division II showing a significant common power in the 2–3 year and

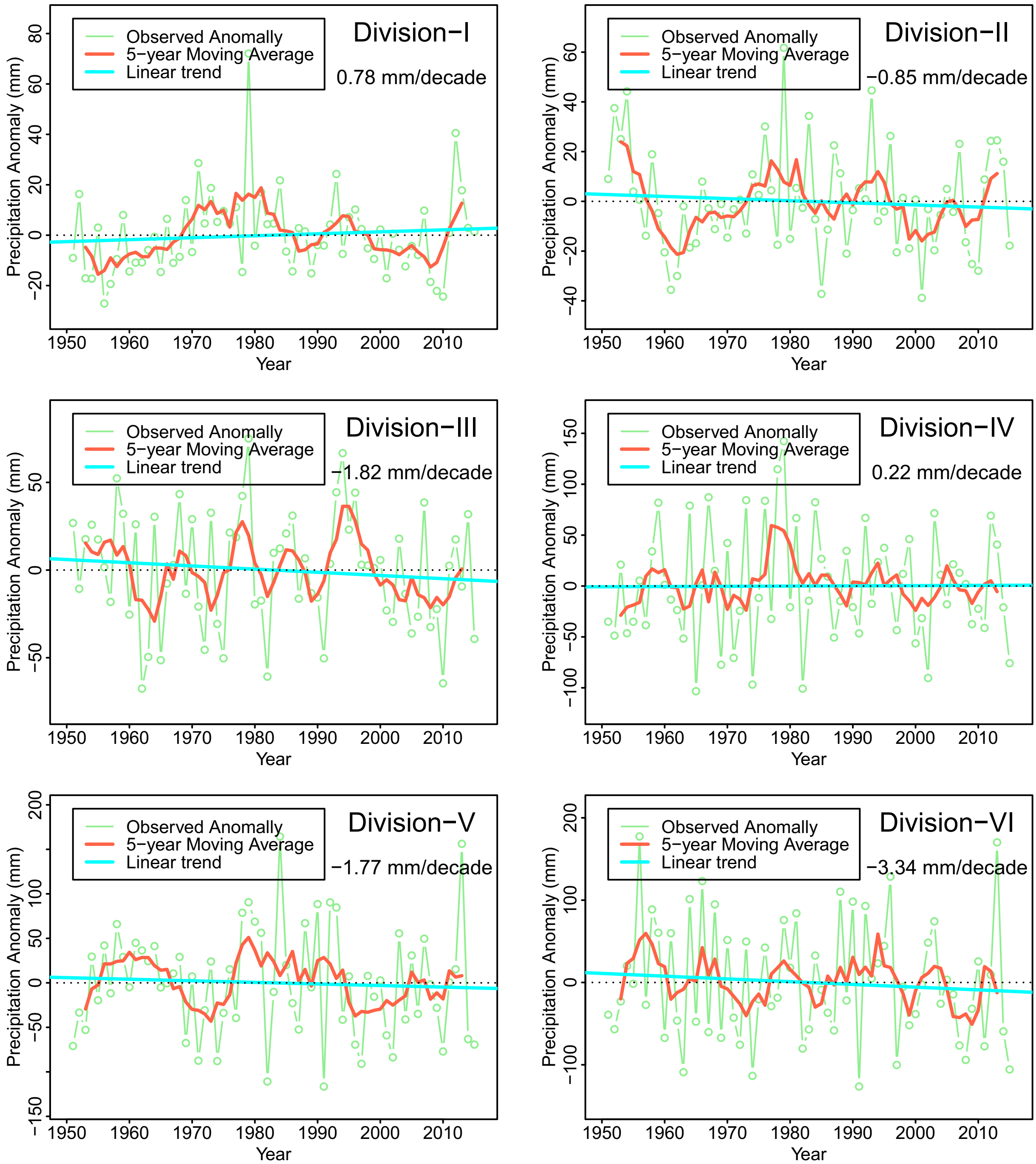

Fig. 9. Time series of regionally averaged summer precipitation anomalies (circles) as well as the linear trends (straight lines) and the 5-year moving averages (the smoother lines).

3–5 year cycle during 1995–2000 and 1975–1990, respectively. Similar patterns of shared power were seen in the cross wavelet transform between EASMI and summer precipitation in Division V (Fig. 14b). The common power in 3–5 year periodicity during 1975–1990 also appeared in the cross wavelet transform between SOI and summer precipitation in Division V (Fig. 14c). This result could also been verified by the common peaks in 3–7 year during 1975–1990. Fig. 14(d) illustrated another significant common power in 7–9 year period from 1975–1995 in the cross wavelet transform between EAWR and summer precipitation in Division III. Other 14 cross wavelet transforms were shown as Supplementary materials.

3.4. Changes in large scale atmospheric circulation

In previous studies, change points of climate extremes were detected in the 1980s (H.X. Wang et al., 2013; H.J. Wang et al., 2013). Our analysis also indicated that rapid warming started in 1980s. To investigate the impact of large scale circulation changes on climate

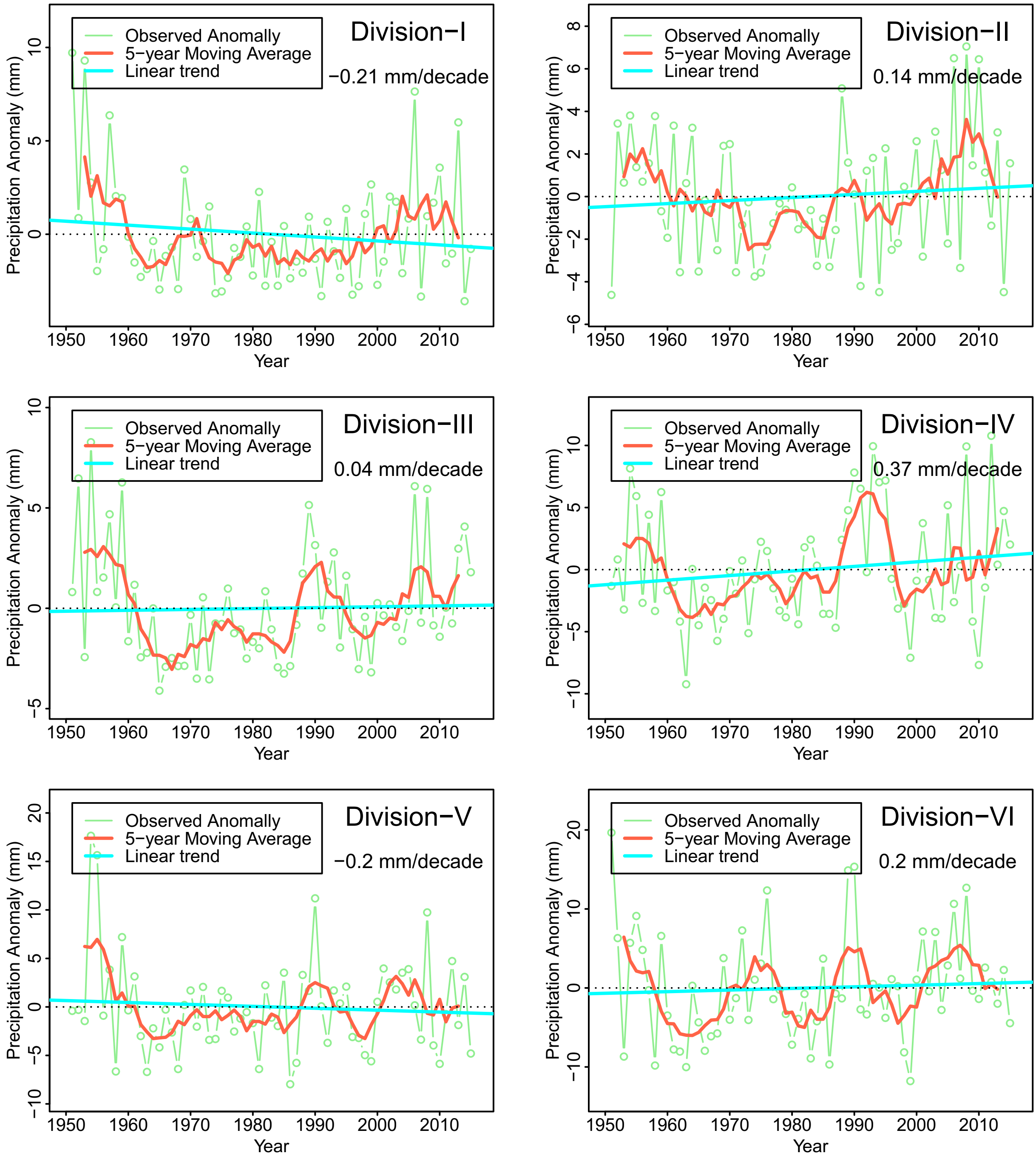

Fig. 10. Time series of regionally averaged winter precipitation anomalies (circles) as well as the linear trends (straight lines) and the 5-year moving averages (the smoother lines).

change, composite circulation maps were created from NCEP/NCAR reanalysis in summer and winter for the periods 1956–1980 and 1981–2015, and the former were subtracted from the latter (new minus old) to represent the variations in circulation between the two periods (Fig. 15). These two seasons were chosen because East Asian Monsoon was most conspicuous in summer and winter influencing the climate over much of China (Ding and Chan, 2005; Zhou et al., 2008). Fig. 15 showed the mean difference of wind vectors and geopotential height at 500 hPa between 1981–2015 and 1956–1980 for summer and winter, respectively. As shown on the geopotential height composite, enhanced anticyclonic circulation developed near Mongolia and the largest differences (approximately 40 gpm) were located at 46°N and 100°E at 500 hPa in summer (Fig. 15a). This suggested a weaker eastern Asian summer monsoon during 1981–2015 as compared to 1956–1980. The increased geopotential height over Mongolia was also consistent with rapid warming in NWC. In winter, an enhanced anticyclonic circulation developed at northern China (near 45°N and 110°E) as seen in the geopotential height composite (Fig. 15b), and an anomalous cyclonic circulation also developed over the Eurasian continent (60°N and 55°E). The differences between anticyclonic circulation and cyclonic

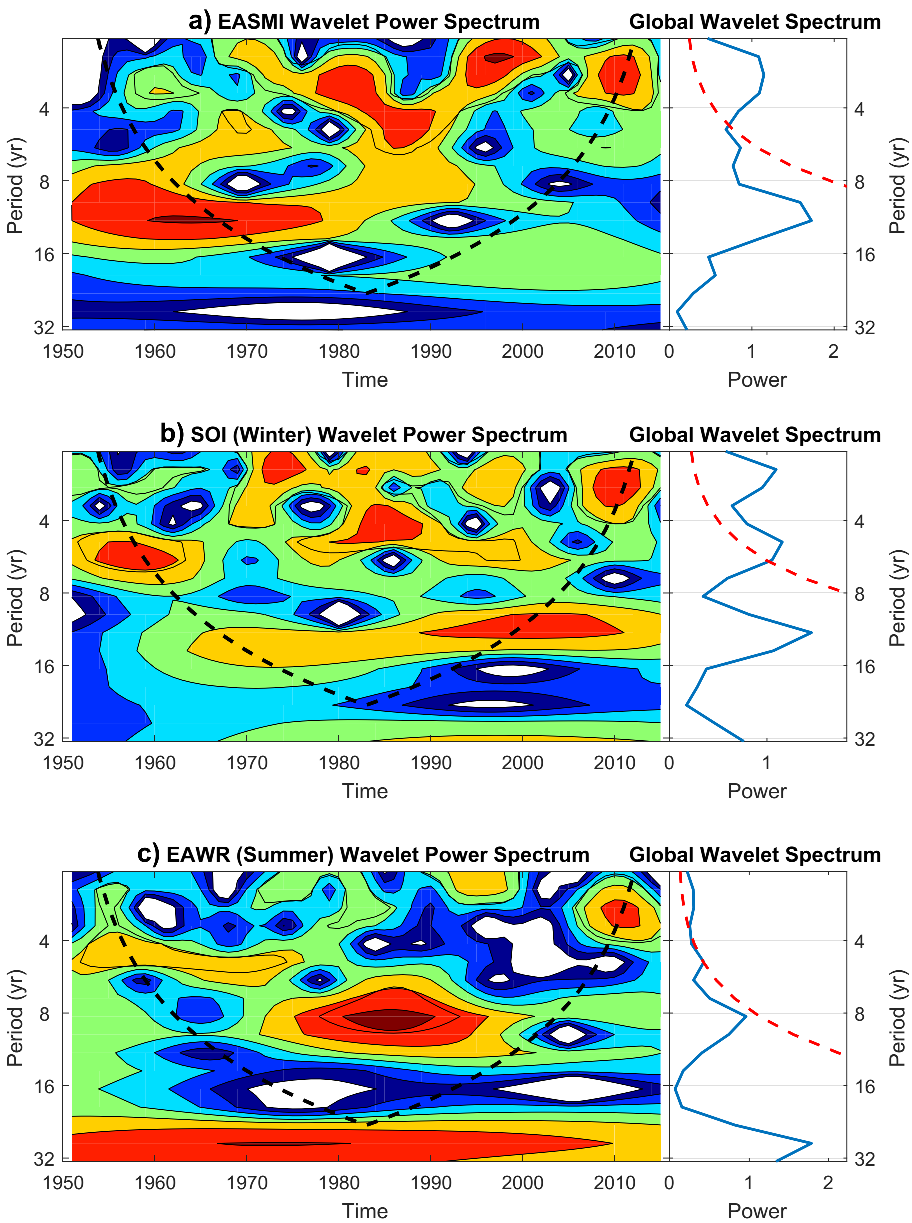

Fig. 11. Continuous wavelet power spectrum and global wavelet spectrum of (a) EASMI, (b) SOI (winter), (c) EAWR (summer) time series from 1951–2015. (The thick black contour designates the 95% confidence level against red noise and the cone of influence (COI) where edge effects might distort is shown as the U-shape line.) (For interpretation of the references to colour in this figure legend, the reader is referred to the web version of this article.)

circulation resulted in an enhanced westerly during 1981–2015 as compared to 1956–1980. Then, the southwesterly wind in northern Mongolia has been strengthened, but the southern extent of winter monsoon has been weakened reducing the incursion of colder air in winter. Rapid warming in NWC in winter since 1980s was mainly attributable to the above change in large scale circulation. Similar characteristics of wind fields and geopotential height are shown at 850 hPa (Supplementary materials).

4. Discussion and conclusions

Gansu Province is located at the important climate transition zone in NWC, and used to be the important landscape corridor connecting agriculture and nomadic civilizations since ancient times. Oasis agriculture based on irrigating arisen in central Gansu with thousands years history. Investigating the spatial and temporal variations of temperature and precipitation is helpful to better understanding regional climate change. Based on daily observation dataset from 29 meteorological stations in Gansu during 1951–2015, the spatial and temporal variability of temperature and precipitation (both extreme and average) were synthetically analyzed in this study.

The trends of climate extremes were firstly investigated using 11 indices of extreme temperature and 4 of extreme precipitation. All the temperature-based extreme climate indices showed patterns consistent with a general warming trend in NWC (Xu et al., 2011; You et al., 2011; Li et al., 2013). Significant increases in warm nights/days and

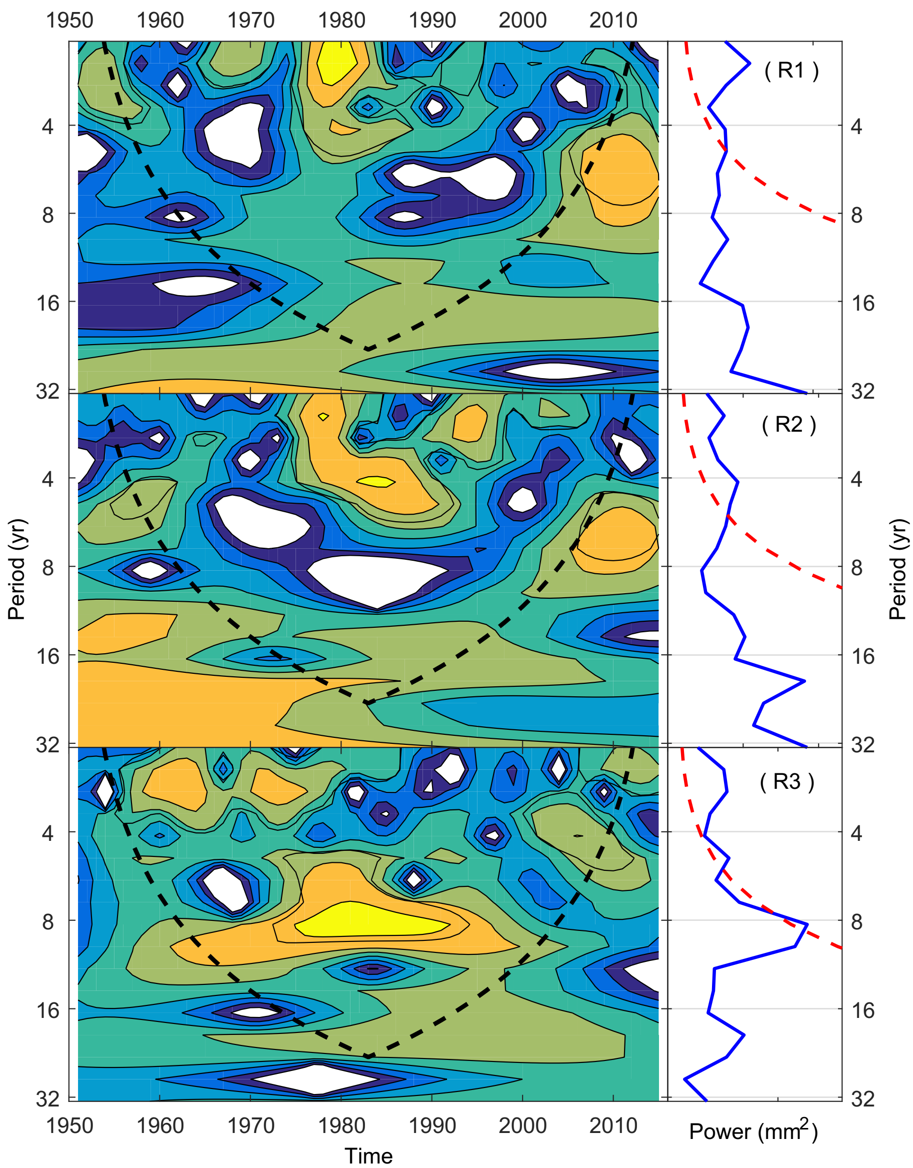

Fig. 12. Continuous wavelet power spectrum and global wavelet spectrum of regionally averaged summer precipitation anomalies from 1951–2015 in Division I, II, and III.

significant decreases in cold nights/days were observed during 1951–2015 at most stations in Gansu. However, the increasing trends in minimum temperature extremes were more rapid than those in maximum temperature extremes, resulting in decreasing DTR (Fig. 2). The warming climate has caused the number of consecutive warm days to increase significantly while the number of consecutive cold days to decrease significantly. The annual mean temperature warmed by 0.13 to 0.42 °C/decade, which was comparable with the China means (0.27 °C/decade; Liu et al., 2004; You et al., 2011). It was worthy to point out that the warming rate near the northeastern margin of Tibetan Plateau with a high altitude reached 0.42 °C/decade. This result was consistent with the rapid warming pattern on the Tibetan Plateau (Wu et al., 2012). For extreme precipitation indices, significant trends were not detected at most stations in Gansu. This finding was in accordance with the trends of annual maximum precipitation revealed in Gao et al. (2016). Moreover, positive trends in extreme precipitation indices were mainly distributed in central and western Gansu belonging to arid region. Similar positive trends in both mean and extreme precipitation were found in the western part of NWC (Wang et al., 2013a; Wang et al., 2013b). However, in this study we found that the change trends in annual and seasonal precipitation were not statistically significant at mot stations in Gansu as expected. So change in precipitation was further analyzed at regional level after spatial grouping of meteorological stations.

Hierarchical clustering method has been applied to implement the spatial grouping of the 29 station in Gansu. The same spatial grouping results for temperature and precipitation indicated that the spatial patterns of temperature and precipitation were consistent in Gansu (Fig. 6). Synchronized heat and moisture was in line with the characteristics of East Asian monsoon climate (Ding and Chan, 2005). Thus, the role of East Asian monsoon on determining the spatial distribution of the summer precipitation in Gansu was also investigated. The regional-averaged annual, summer, and winter mean temperature anomalies showed a significant increasing trend in all 6 Divisions

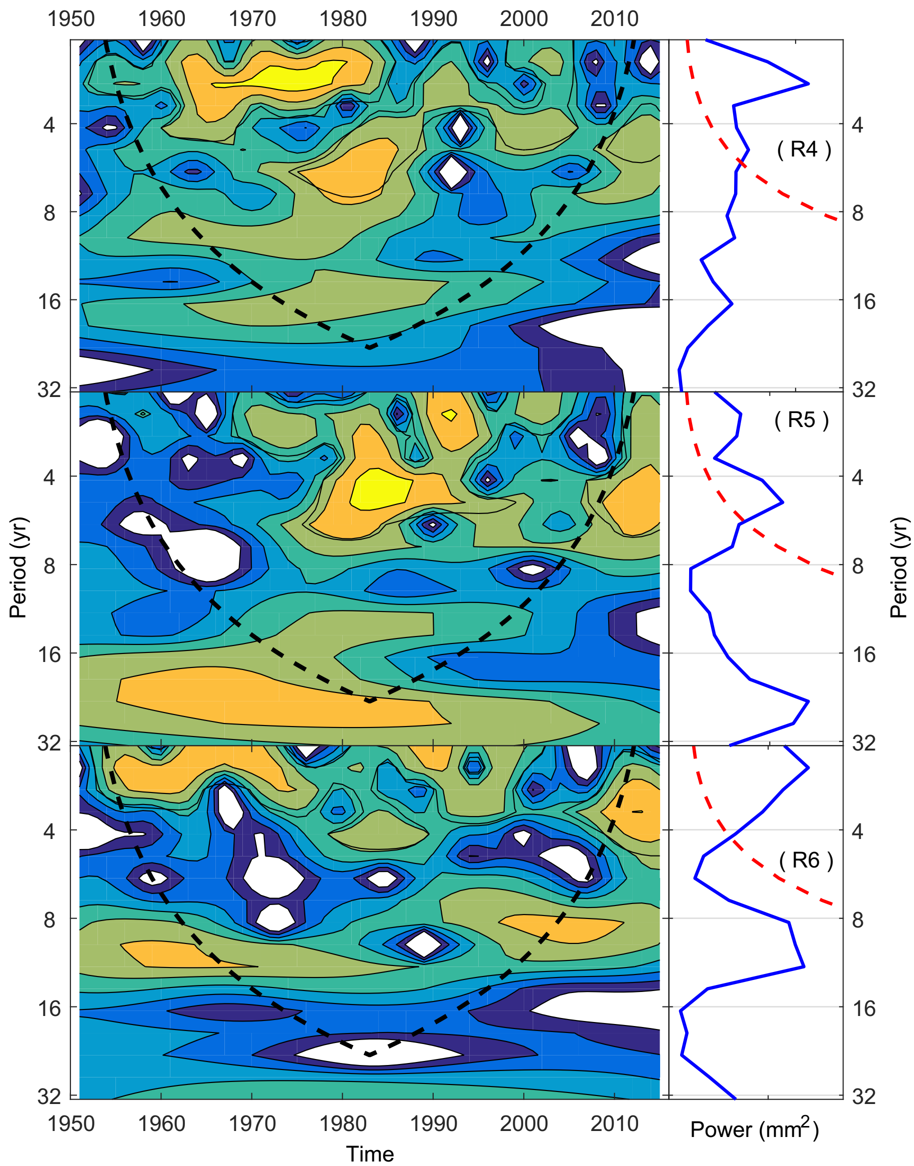

Fig. 13. Continuous wavelet power spectrum and global wavelet spectrum of regionally averaged summer precipitation anomalies from 1951–2015 in Division IV, V, and VI.

during the last 65 years (Fig. 7). The rapid increasing of mean temperature began at the end of 1970s that was close to the transition point of climate change around 1983 in NWC (Qian and Qin, 2008). Linear trend analysis showed that annual total precipitation increased in the western part of Gansu but decreased in the eastern part belonging to the Loess Plateau. In the past few years, there has been a lot of research focusing on the climate change on Loess Plateau showing a warming and drying trend (Li et al., 2010; Wang et al., 2012; Sun et al., 2016; Wang et al., 2016). In other references, regional differences of trends in precipitation in NWC were also identified that annual total precipitation only increased in the western part of NWC but decreased in the eastern part of NWC (Fu et al., 2013; Han et al., 2016). The spatial variation of annual total precipitation in Gansu was consistent with that in the whole NWC (Han et al., 2016).

The possible attributions of trend and variability of temperature and precipitation in NWC include many large scale atmospheric circulation patterns. East Asian Monsoon, which is divided into a warm and wet summer monsoon and a cold and dry winter monsoon, determines the spatiotemporal variability of summer rainfall over China (Ding and Chan, 2005; Zhao and Zhou, 2009). In this study, we found that the inter-decadal teleconnection between EASMI and summer precipitation were statistically significant (see Supplementary materials). ENSO also impacts the yearly variability of the global climate including temperature and summer precipitation in China (Tanaka, 1997; Wang et al., 2000). It was found that there existed significant inter-decadal teleconnection between ENSO and extreme precipitation in NWC (Fu et al., 2013). The teleconnection between ENSO and summer precipitation was also verified in this study. EAWR is one of predominant Northern Hemisphere teleconnection pattern that influences wet season precipitation in Xinjiang, NWC (Tan and Shao, 2016). The cross wavelet transform between EAWR and summer precipitation in the Division-III showed a significant common power 7–11 year period during

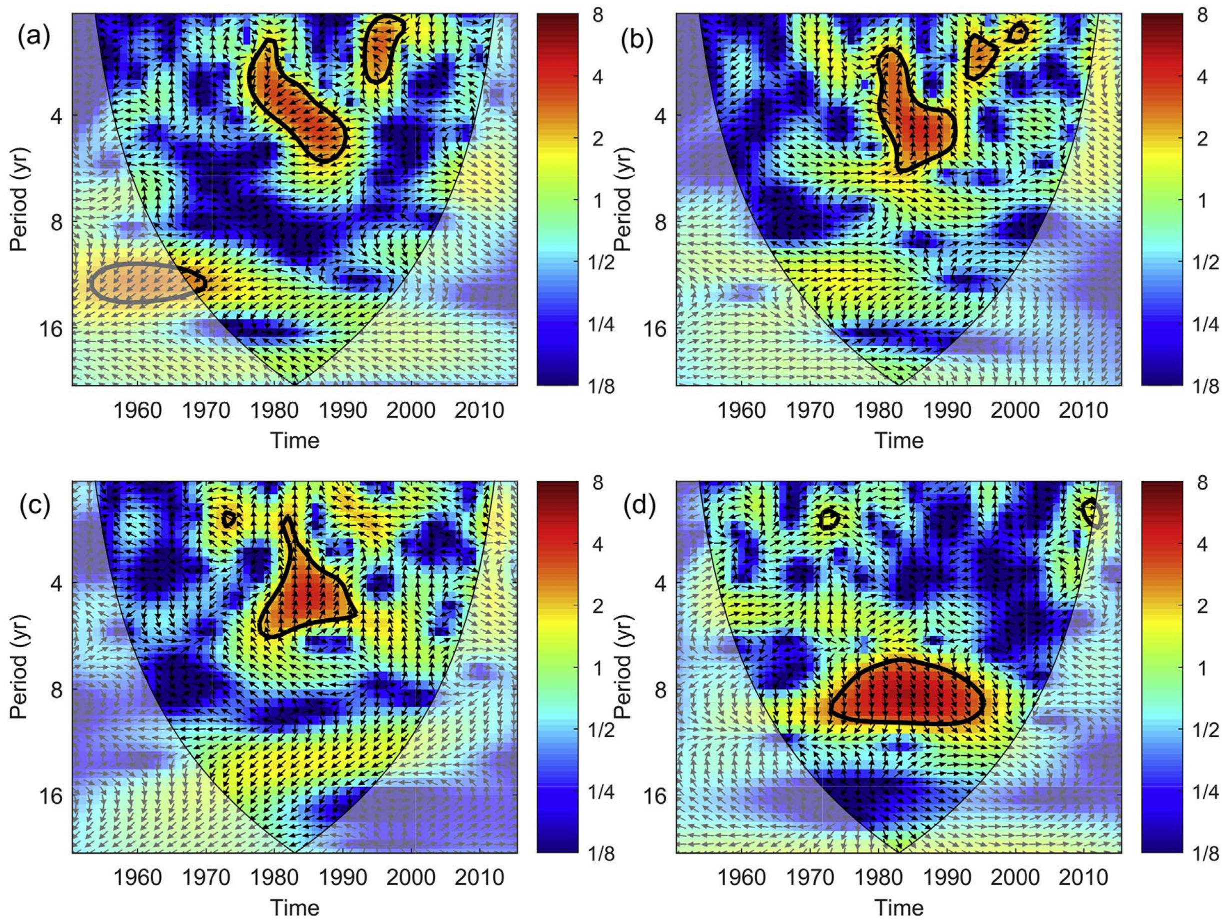

Fig. 14. Cross wavelet transform of (a) EASMI and summer precipitation in Division II, (b) EASMI and summer precipitation in Division V, (c) SOI and summer precipitation in Division V, and (d) EAWR and summer precipitation in Division III. (The thick black contours depict the 5% significance level of local power relative to red noise, and the black line is the cone of influence. Right-pointing arrows indicate that the two signals are in phase while left-pointing arrows are for anti-phase signals.) (For interpretation of the references to colour in this figure legend, the reader is referred to the web version of this article.)

1970–1995. In general, the wavelet analyses revealed that the teleconnection between large scale circulation and summer precipitation varied not only from region to region, but also was different at different time scale and different time periods. We note that large scale circulation patterns those might influence spatial variations of summer precipitation in Gansu are not limited to EASMI, SOI, and EAWR. As a matter of fact, the relationships between large scale circulation pattern and summer precipitation in NWC are much more complicated than that revealed in this study.

The composite circulation maps have clearly revealed the impact of large scale circulation changes on regional climate change. In summer, the enhanced geopotential height over northern China and Mongolia suggested a weaker eastern Asian summer monsoon during 1981–2015 as compared to 1956–1980. It has prevented northward transportation of water vapor flux and limited moisture propagation to northern China. In winter, the southwesterly wind in northern Mongolia has been strengthened due to enhance anticyclonic circulation and anomalous cyclonic circulation over the Eurasian continent, in turn weakened the southern extent of the winter monsoon. The above changes in large scale circulation were attributable to the rapid warming and changing in precipitation in Gansu, NWC. Besides atmospheric circulation abnormities, terrain might be another major reason resulting in the spatial variation characteristics in temperature and precipitation over Gansu Province. The territory of Gansu Province is long and narrow spanning > 1400 km from southeast to northwest. As a representative climate transition zone in NWC, it is worthy to investigate the spatial and temporal variabilities in temperature and precipitation as well as the underlying mechanisms of climate change in the future. In particular, under the circumstance of rapid warming and drying, more attentions should be paid on drought in Gansu, NWC.

Acknowledgement

This work was partly supported by the Youth Innovation Promotion Association, CAS (2016195), Key Research Program of Frontier Sciences of CAS (QYZDJ-SSW-DQC031), CAS Knowledge Innovation Project (KZCX2-EW-QN209), S & T Service Network Initiative (KFJ-EW-STS-127-2), and National Natural Science Foundation of China (31570423). The authors appreciate the Climate Data Center of the CMA for providing the meteorological data. Helpful comments from the anonymous reviewer and editor are also acknowledged.

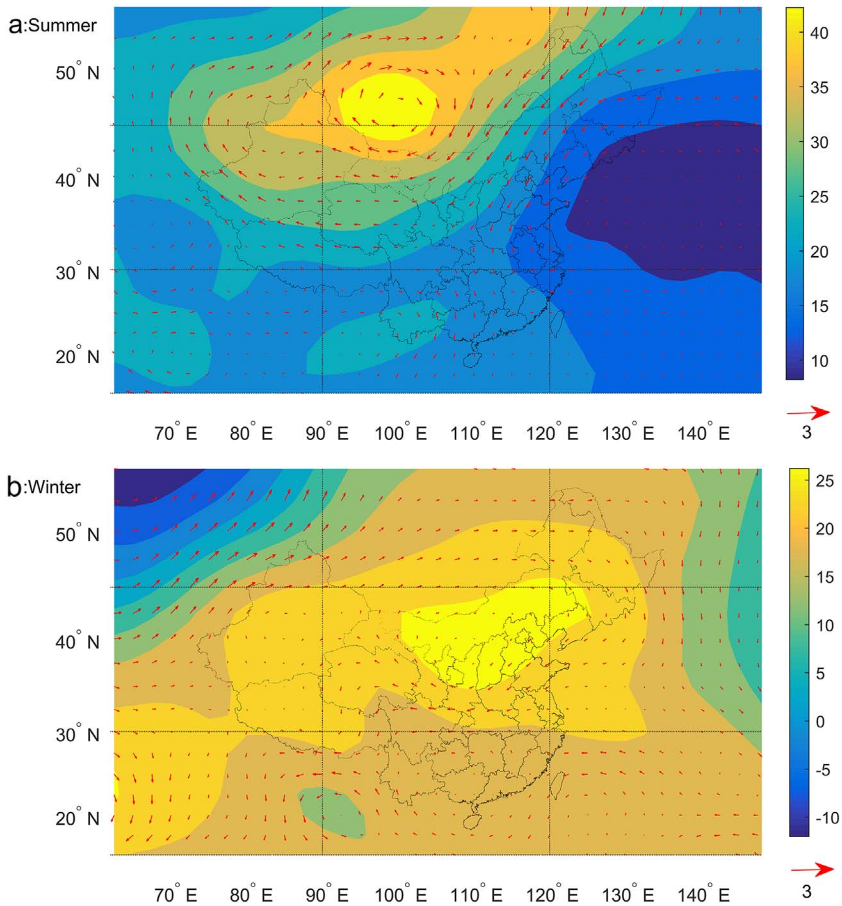

Fig. 15. Difference of wind speed and geopotential height at 500 hPa in summer (top) and winter (bottom) between 1981–2015 and 1956–1980.

Appendix A. Supplementary materials

Supplementary materials to this article can be found online at http://dx.doi.org/10.1016/j.atmosres.2017.07.001.

References

Alexander, L., Zhang, X., Peterson, T., Caesar, J., Gleason, B., Klein Tank, A., Haylock, M., Collins, D., Trewin, B., Rahimzadeh, F., 2006. Global observed changes in daily climate extremes of temperature and precipitation. J. Geophys. Res. Atmos. 111, D05109.

Beniston, M., Diay, H.F., Bradley, R.S., 1997. Climate change at high elevation sites: an overview. Clim. Chang. 36, 233–251.

Brohan, P., Kennedy, J.J., Harris, I., Tett, S.F.B., Jones, P.D., 2006. Uncertainty estimates in regional and global observed temperature change: a new data set from 1850. J. Geophys. Res. Atmos. 111, D12106.

Burn, D.H., HagElnur, M.A., 2002. Detection of hydrological trend and variability. J. Hydrol. 255, 107–122.

Chen, G., Huang, R., 2012. Excitation mechanisms of the teleconnection patterns affecting the July precipitation in Northwest China. J. Clim. 25 (22), 7834–7851.

Diaz, H.F., Grosjean, M., Graumlich, L., 2003. Climate variability and change in high elevation regions: past, present and future. Clim. Chang. 59, 1–4.

Ding, Y.H., Chan, J.C.L., 2005. The East Asian summer monsoon: an overview. Meteorog. Atmos. Phys. 89, 117–142.

Ding, Q., Wang, B., 2005. Circumglobal teleconnection in the Northern Hemisphere summer. J. Clim. 18 (17), 3483–3505.

Easterling, D.R., Meehl, G.A., Parmesan, C., Changnon, S.A., Karl, T.R., Mearns, L.O., 2000. Climate extremes: observations, modeling and impacts. Science 289, 2068–2074.

Fu, G., Yu, J., Yu, X., Ouyang, R., Zhang, Y., Wang, P., Liu, W., Min, L., 2013. Temporal variation of extreme rainfall events in China, 1961–2009. J. Hydrol. 487, 48–59.

Gao, M., Mo, D., Wu, X., 2016. Nonstationary modeling of extreme precipitation in China. Atmos. Res. 182, 1–9.

Gay-Garcia, C., Estrada, F., Sanchez, A., 2009. Global and hemispheric temperatures revisited. Clim. Chang. 94, 333–349.

Grinsted, A., Jevrejeva, S., Moore, J., 2004. Application of the cross wavelet transform and wavelet coherence to geophysical time series. Nonlinear Process. Geophys. 11, 561–566.

Han, X., Xue, H., Zhao, C., Lu, D., 2016. The roles of convective and stratiform precipitation in the observed precipitation trends in Northwest China during 1961–2000. Atmos. Res. 169, 139–146.

Hansen, J., Sato, M., Ruedy, R., Lo, K., Lea, D.W., Medina-Elizade, M., 2006. Global temperature change. Proc. Natl. Acad. Sci. U. S. A. 103 (39), 14288–14293.

Hosking, J.R.M., Wallis, J.R., 1997. Regional Frequency Analysis: An Approach Based on L-Moments. Cambridge University Press, Cambridge, UK.

Houghton, T.J., Ding, Y., Griggs, D.J., Noguer, M., van der Linden, P.J., Dai, X., Maskell, K., Johnson, C.A., 2001. Climate Change 2001: The Science Basis. Cambridge University Press, Cambridge, New York.

Huang, G., Liu, Y., Huang, R., 2011. The interannual variability of summer rainfall in the arid and semiarid regions in Northern China and its association with the Northern Hemisphere circumglobal teleconnection. Adv. Atmos. Sci. 28 (2), 257–268.

Huntington, T.G., 2006. Evidence for intensification of the global water cycle: review and synthesis. J. Hydrol. 319 (1–4), 83–95.

IPCC, 2007. Summary for policymakers. In: Solomon, S., Qin, D., Manning, M., Chen, Z., Marquis, M., Averyt, K.B., Tignor, M., Miller, H.L. (Eds.), Climate Change 2007: The Physical Science Basis, Contribution of Working Group I to the Forth Assessment Report of the Intergovernmental Panel on Climate Change. Cambridge University Press, Cambridge, New York.

IPCC, 2012. Special report on managing the risks of extreme events and disasters to advance climate change adaptation. In: A Report of Working Groups I and II of the Intergovernmental Panel on Climate Change. Cambridge University Press, Cambridge, New York.

IPCC, 2014. Climate change 2014: synthesis report. In: Contribution of Working Groups I, II and III to the Fifth Assessment Report of the Intergovernmental Panel on Climate Change. Cambridge University Press, Cambridge, New York.

Kendall, M.G., 1970. Rank Correlation Methods. Griffin, London.

Klein Tank, A.M.G., Wijngaard, J., Können, G.P., Petrovic, P., 2002. Daily surface air temperature and precipitation dataset 1901–1999 for European Climate Assessment (ECA). Int. J. Climatol. 22, 1441–1453.

Klein Tank, A.M.G., Peterson, T.C., Quadir, D.A., Dorji, S., Zou, X., Tang, H., Santhosh, K., Joshi, U.R., Jaswal, A.K., Kolli, R.K., Sikder, A.B., Deshpande, N.R., Revadekar, J.V., Yeleuova, K., Vandasheva, S., Faleyeva, M., Gomboluudev, P., Budhathoki, K.P., Hussain, A., Afzaal, M., Chandrapala, L., Anvar, H., Amanmurad, D., Asanova, V.S., Jones, P.D., New, M.G., Spektorman, T., 2006. Changes in daily temperature and precipitation extremes in central and south Asia. J. Geophys. Res. 111, D16.

Li, Z., Zheng, F.L., Liu, W.Z., Flanagan, D.C., 2010. Spatial distribution and temporal trends of extreme temperature and precipitation events on the Loess Plateau of China during 1961–2007. Quat. Int. 226, 92–100.

Li, B.F., Chen, Y.N., Shi, X., Chen, Z.S., Li, W.H., 2013. Temperature and precipitation changes in different environments in the arid region of northwest China. Theor. Appl. Climatol. 112, 589–596.

Li, B.F., Chen, Y.N., Chen, Z.S., Xiong, H.G., Lian, L.S., 2016. Why does precipitation in northwest China show a significant increasing trend from 1960 to 2010? Atmos. Res. 167, 275–284.

Lim, Y.-K., 2015. The East Atlantic/West Russia (EA/WR) teleconnection in the North Atlantic: climate impact and relation to Rossby wave propagation. Clim. Dyn. 44 (11 – 12), 3211–3222.

Limsakul, A., Singhruck, P., 2016. Long-term trends and variability of total and extreme precipitation in Thailand. Atmos. Res. 169, 301–317.

Lin, L., Lu, R., 2009. The ENSO's effect on eastern China rainfall in the following early summer. Adv. Atmos. Sci. 26 (2), 333–342.

Liu, B.H., Xu, M., Henderson, M., Qi, Y., Li, Y.Q., 2004. Taking China's temperature: daily range, warming trends, and regional variations, 1955–2000. J. Clim. 17 (22), 4453–4462.

Mann, H.B., 1945. Nonparametric test against trend. Econometrica 13, 245–259.

New, M., Todd, M., Hulme, M., Jones, P., 2001. Precipitation measurements and trends in the twentieth century. Int. J. Climatol. 21 (15), 1889–1922.

Panda, D.K., Panigrahi, P., Mohanty, S., Mohanty, R.K., Sethi, R.R., 2016. The 20th century transitions in basic and extreme monsoon rainfall indices in India: comparison of the ETCCDI indices. Atmos. Res. 181, 220–235.

Qian, W., Lin, X., 2005. Regional trends in recent temperature indices in China. Meteorog. Atmos. Phys. 90, 193–207.

Qian, W.H., Qin, A., 2008. Precipitation division and climate shift in China from 1960 to 2000. Theor. Appl. Climatol. 93, 1–17.

Revi, A., Bazaz, A., Krishnaswamy, J., Bendapudi, R., D'Souza, M., Pahwa Gajjar, S., 2015. Vulnerability and adaptation to climate change in semi-arid areas in India. In: ASSAR Working Paper. ASSAR PMU, South Africa.

Sarr, B., 2012. Present and future climate change in the semi-arid region of West Africa: a crucial input for practical adaptation in agriculture. Atmos. Sci. Lett. 13 (2), 108–112.

Sun, W., Mu, X., Song, X., Wu, D., Cheng, A., Qiu, B., 2016. Changes in extreme temperature and precipitation events in the Loess Plateau (China) during 1960–2013 under global warming. Atmos. Res. 168, 33–48.

Tan, X., Shao, D., 2016. Precipitation trends and teleconnections identified using quantile regressions over Xinjiang, China. Int. J. Climatol.. http://dx.doi.org/10.1002/joc.4794. (in press).

Tanaka, M., 1997. Interannual and interdecadal variation of the western north Pacific monsoon and the East Asian Baiu rainfall and their relationship to enso cycle. J. Meteor. Soc. Japan 75, 1109–1123.

Torrence, C., Webster, P.J., 1999. Inter decadal changes in the ENSO-Monsoon system. J. Clim. 12, 2679–2690.

Trenberth, K.E., 1997. The definition of El Niño. Bull. Am. Meteorol. Soc. 78, 2771–2777.

Trenberth, K.E., 2011. Changes in precipitation with climate change. Clim. Res. 47, 123–138.

Wang, B., Wu, F., Fu, X., 2000. Pacific-east Asian teleconnection: how does ENSO affect east Asian climate? J. Clim. 13, 1517–1536.

Wang, Q.X., Fan, X.H., Qin, Z., Wang, M., 2012. Change trends of temperature and precipitation in the Loess Plateau Region of China, 1961–2010. Glob. Planet. Chang. 92-93, 138–147.

Wang, H.X., Liu, X., Li, C., Ren, Z., Pan, D., Wei, J., 2013a. Spatial-temporal distribution of precipitation in Gansu Province last 42 years. Chin. J. Agrometeorol. 34 (4), 384–389. http://dx.doi.org/10.3969/j.issn.1000-6362.2013.04. 002. (in Chinese with English abstract).

Wang, H.J., Chen, Y.N., Chen, Z.S., 2013b. Spatial distribution and temporal trends of mean precipitation and extremes in the arid region, northwest of China, during 1960–2010. Hydrol. Process. 27, 1807–1818.

Wang, Q.X., Wang, M., Fan, X.H., Zhang, F., Zhou, S.Z., Zhang, T., 2016. Trends of temperature and precipitation extremes in the Loess Plateau Region of China, 1961–2010. Theor. Appl. Climatol.. http://dx.doi.org/10.1007/s00704-016-1820-z. (in press).

Wu, S., Lu, A., Li, L., 2012. Spatial and temporal characteristics of minimum temperature in winter in China during 1961–2010 from NCEP_NCAR reanalysis. Theor. Appl. Climatol. 108, 207–216.

Xinhua News, 2015. http://news.xinhuanet.com/politics/2015-06/18/c_1115663573.html (accessed 17.06.25).

Xu, X., Du, Y., Tang, J., Wang, Y., 2011. Variations of temperature and precipitation extremes in recent two decades over China. Atmos. Res. 101, 143–154.

Yan, Z., Jones, P.D., Davies, T.D., Moberg, A., Bergström, H., Camuffo, D., Cocheo, C., Maugeri, M., Demare, G.R., Verhoeve, T., Thoen, E., Barriendos, M., Rodrıguez, R., Martn-Vide, J., Yang, C., 2002. Trends of extreme temperatures in Europe and China based on daily observations. Clim. Chang. 53, 355–392.

Yang, P., Xia, J., Zhang, Y.Y., Honh, S., 2017. Temporal and spatial variations of precipitation in Northwest China during 1960–2013. Atmos. Res. 183, 283–295.

You, Q.L., Kang, S.C., Aguilar, E., Pepin, N., Flügel, W.A., Yan, Y.P., Xu, Y.W., Zhang, Y.J., Huang, J., 2011. Changes in daily climate extremes in China and its connection to the large scale atmospheric circulation during 1961–2003. Clim. Dyn. 36, 2399–2417.

Zhao, P., Zhou, Z.J., 2009. An East Asian subtropical summer monsoon index and its relationship to summer rainfall in China. Acta Meteorol. Sin. 23, 18–28.

Zhou, X.Y., Ding, Y.H., Wang, P.X., 2008. Moisture transport in Asian summer monsoon region and its relationship with summer precipitation in China. Acta Meteorol. Sin. 66, 59–70.